Author version: Marine Geology: 267(1-2); 2009; 71-85

Shallow gas charged sediments off the Indian west coast: Genesis and distribution.

A. Mazumdar*, A. Peketi, P. Dewangan, F. Badesab, T. Ramprasad, M.V. Ramana
[1]National Institute of Oceanography, Donapaula, Goa-403004, India.

D. J. Patil, A. Dayal,
[2]National Geophysical Research Institute, Kachiguda, Hyderabad-500007, India.

* for correspondence

Abstract
Geophysical and geochemical surveys were carried out off Goa, central west coast of India, to understand the genesis and distribution of shallow gases in marine sediments. Shallow gas charged sediments within the water depths of ~15 to 40 m are reported all along the west coast and are characterized by gas masking, high amplitude and reverse polarity reflections in high resolution seismic (sparker) data, attributed to the presence of free gas. These high amplitude reflections (gas front) are observed within a Holocene fine grained, wedge shaped sediment package overlying the maximum flooding surface. The gas front lies between 1.2 and 5 m below the seabed and demarcates the transition from gas in the dissolved phase to bubble phase when the gas concentration exceeds the saturation level. The observed and extrapolated sulfate methane transition zone (SMTZ) lies between 0.7 and 2.25 m below the seabed and it is related to the depth of the gas front. Methane concentration reaches saturation below the SMTZ, and produce a bubble phase which lowers the p-wave velocity and produces high amplitude reflection observed in the seismic data. Depleted carbon isotope ratios as low as -88.9‰ suggest a microbial origin for the methane in the study area. High sulfate reduction rate, high concentrations of pore-water methane, phosphate and ammonium in the shallowest site (Sasu123/1 at 14.7 m water depth) suggest an enhanced availability of reactive organic matter required for microbially mediated biodegradation processes. High gas flux in the shallow waters is also indicated by the shallowing of the gas front and the widening of the gas masked zone towards shore. The present investigations do not testify the origin of Holocene shallow gases either from buried channel deposits or the Pleistocene sediments.

Key Words. Shallow gases, gas masking, enhanced reflection, methane, and sulfate reduction

* For correspondence: maninda@nio.org

1. Introduction

Gas charged sediments and gas seepages have been reported from the coastal environment all over the world (Fleischer et al., 2001) and methane is the predominant gas found in the shallow marine sediments (Floodgate and Judd, 1992). CO_2 and H_2S are other gas phases commonly recorded in the marine sediments. Hovland and Judd (1992) estimated global annual flux of about $145x10^{12}$ g CH_4 from the shallow gases up to a water depth of 250 m. Compilation of global distribution of shallow gases by Fleischer et al. (2001) shows that most occurrences are typically shallower than 50 m water depth. Apart from the marine environment, numerous occurrences of shallow gases have also been reported from estuaries, coastal lagoons and bays (Kindinger et al., 1994; Vogt et al., 2000; Hobbs, 2004; Liu et al., 2004; García-García et al., 2005; Diez et al., 2007b; Durán et al., 2007; García-García et al., 2007; Iglesias and García-Gil, 2007; Laier and Jensen, 2007). Gassy sediments are commonly found in shallow and productive environments that receive high fluxes of reactive organic matter. Complex, bacterially mediated biogeochemical reactions result in the production of methane in marine sediments (Floodgate and Judd, 1992; Megonigal et al., 2003; Canfield et al., 2005; Reeburgh, 2007).

Methane being a potent greenhouse gas (Lashof and Ahuja, 1990; Judd, 2003) and an efficient energy source (Nakicenovic, 2002), its genesis and occurrence in shallow marine sediments is a topic of wide interest. Moreover, gases in marine sediments are also known to alter significantly the geotechnical properties by reducing shear strength of seabed (Sills and Wheeler, 1992).

Methane may exist as free gas in the pore space and/or as dissolved gas in the solution. The solubility of methane in porewaters depends on bottom water temperature, hydrostatic pressure and salinity (Yamamoto et al., 1976; Duan and Mao, 2006). The size and shape of methane gas bubble in sediments depend on the gas concentrations and nature of sediment (Wilkens and Richardson, 1998; Boudreau et al., 2005; Robb et al., 2006). When present as gas bubble, even at low concentrations (~0.1% free gas content), methane can dramatically decrease the compressional wave velocity, increase the compressional wave attenuation, and increase the sound scattering (Yuan et al., 1992;

Wilkens and Richardson, 1998; Missiaen et al., 2002). Therefore, gas rich sediment layers attenuate the acoustic energy causing the lack of penetration, which results in masking/turbidity and disappearance of underlying depositional features in the seismic data (Judd and Hovland, 1992; Taylor, 1992; Judd and Hovland, 2007).

Siddiquie et al. (1981), Karisiddaiah et al. (1993; 2002), and Karisiddaiah and Subba Raju (2002) have reported occurrences of shallow gases manifested in the form of acoustic masking and turbidity on seismic data along the inner shelf of the west coast of India. In the present work we have carried out detailed geochemical investigations under the constraints of high resolution sparker reflection seismic records of shallow sediments off the coast of Goa (west coast of India) and proposed a coherent picture to understand the genesis of the gas charged sediments. We have attempted to address the issues related to: (i) origin of methane gas in the sediments, (ii) organic matter sources in shallow waters and, (iii) sediment accumulation pattern and factors responsible for localization of gas in the sediment.

2. Geological Framework

The western continental shelf of India occupies an area of about 0.3×10^6 km^2. The continental shelf slopes gently to the west with a gradient of 1:400 to 1:3000 to a water depth of 140 m. The inner shelf is marked by an even and gentle topography with a slope of 1:700 to 1:3300 (Wagle et al., 1994). The inner shelf is covered by silt and clay up to a water depth of 50 m and by calcareous sands beyond this depth up to shelf break (Nair and Pylee, 1968; Nair et al, 1978). The width of the clay and silt rich cover ranges from 175 km off Narmada-Tapti in the north to ~25 km off Cochin in the south (Rao and Wagle, 1997). Silty clays and/or laminated olive grey to dark brown mud occur on the middle shelf to slope region (Rao and Veerayya, 2000). Karisiddaiah et al. (2002) and Ramprasad et al. (2005) recognized several seismic units including buried channels within the late-Quaternary deposits on the western Indian shelf, described various system tracts and attempted to put them in a chronological framework.

3. Methodology

3.1 Geophysical and Geological

High resolution seismic data was acquired onboard CRV Sagar Sukti (Sasu 75) using an Applied Acoustics CSP1000J Sparker System. The sparker system consists of a power supply with an output power of 100 to 1000 J/sec which is supplied to a multi tipped sparker frame towed at the stern of the ship. The sparker generates a sound pulse (dominant frequency of 800 to 1000 Hz) that travels through the water column, seabed and subsurface sediments and reflects back to the sea surface. The reflected acoustic signal is received by a single channel streamer consisting of an array of hydrophones and sent to the Octopus 360 Data Acquisition System. The recorded digital data has been processed using ProMAX software. The DGPS – NT300D Receiver was deployed to obtain positions along the seismic lines during survey.

Eight 1.27 to 1.95 m long gravity cores and 27 grab samples were collected from the water depths of 14.5 to 47 m (Figure 1). Gravity core locations were selected based on high resolution seismic reflection data, which depicted zones of gas masking of shallow subsurface. As far as possible, cores were collected close to the seismic survey lines. Acrylic liners (2 m x 5.5 cm) were used for collection of gravity cores. In some of the cores the top few cm were lost during core retrieval. Core locations and water depths are shown in Table 1.

Gamma density of the whole core was measured using a GEOTEK Multisensor Core Logger (MSCL) following standard GEOTEK calibration protocol (GEOTEK MSCL Manual, 2000). The bulk density of the sediment was measured using the gamma ray source (Caesium-137) and detector mounted across the core. A narrow beam of gamma rays is emitted from a source with energies principally at 0.662 MeV. These photons pass through the core and are detected on the other side. At this energy level the primary mechanism for the attenuation of gamma rays is by Compton scattering. The incident photons are scattered by the electrons in the core with a partial energy loss. The attenuation, therefore, is directly related to the bulk density of the sediment. The porosity (ϕ) can be derived from the bulk density (ρ_{MSCL}) assuming that the sediment is fully

saturated with water and the known grain (ρ_s = 2.65 g/cc) and fluid (ρ_{fl} = 1.03 g/cc) densities using the following relationship:

$$\rho_{MSCL} = \phi\rho_{fl} + (1-\phi)\rho_s \qquad \textbf{Eq.1}$$

Grain size analyses were carried out by standard gravitational settling method (Tucker, 1998).

3.2 Geochemical

The sediment sub-sampling for gas and pore-water extraction was carried out as 5-10 cm slices within 20-30 minutes of core retrieval. Measured sediment lengths were extruded from the liner using a piston, and cut into slices. Gas sampling was carried out from fresh sediment surface using a 10 ml cut syringe, which can be penetrated deep inside the sediment to avoid contamination. Such subsamples were stored in 28 ml glass vials with 10 ml of anti-bacteriacide chemical and crimped immediately following nitrogen flushing. All the sediment samples were homogenized using a vortex shaker and stored at 2°C. Methane concentrations in the head space were then measured using a Varian Gas chromatograph (CP 3380).

Each sub-sampled core slab was kept in a plastic bag, flushed with nitrogen, sealed and stored at 2°C. Pore water was extracted from the sediment using a cryocentrifuge (Heraus Biofuge maintained at 4°C). The pore water was filtered through 0.2 micron Whatman syringe filter and stored in crimp vials under nitrogen head, and preserved at 2°C for measurement of total alkalinity (TA), pH, sulfate, ammonium and phosphate concentrations. Sulfate concentrations were measured using a Dionex-600 ion chromatograph. Prior to sample injection, 1 ml of pore water sample was diluted to 50 ml or 100 ml and passed through sliver cartridge to remove chloride ion. An IonPac AS9-HC column was used for ion separation, and an ASRS UltraII (2 mm) was used as anion self-regenerating suppressor. The calibration curve was prepared using standard IC sulfate solution from Dionex. Total alkalinity (TA) and pH were measured using a Metrohm Autotitrator (Titrino 799GPT). A micro glass electrode was used for pH measurement and 0.1 N suprapure HCL was used for alkalinity titration. Ammonium and phosphate concentrations were measured using a standard colorimetric technique (Gieskes et al., 1991).

Total carbon (TC) and total nitrogen (TN) content of the sediments were measured with elemental analyzer (Thermo CNS 2500). Approximately 8-10 mg of powdered sediment samples were packed in tin cups and combusted at 1050 ºC and 950 ºC in oxidation and reduction columns respectively with helium as carrier gas. CO_2 and N_2 were detected by TCD detector. Total inorganic carbon (TIC) was measured using UIC carbon coulometer (CM 5130). Total organic carbon (TOC) was calculated by subtracting TIC from TC.

Carbon stable isotope ratio measurement of the head space gases and organic carbon was carried out using a Thermo-Finnigan Delta Plus continuous flow isotope ratio mass spectrometer attached with a gas chromatograph. The external precision calculated is typically 0.07–0.09 ‰ for $\delta^{13}C$. The carbon isotope ratios are reported in standard $\delta^{13}C$ format relative to VPDB standard.

3.2 Computational

Diffusive flux (J) of sulfate was calculated from the concentration profiles using Fick's First law (Eq-1) and steady state conditions (Berner, 1980; Canfield, 1989, 1991),

$$J = \varphi D_s (dC/dX) \qquad \textbf{Eq-2}$$

where, J (mmol cm^{-2} yr^{-1}) is equivalent to the depth-integrated sulfate reduction rate and C is the sulfate concentration (mmol cm^{-3}) in the pore water. dC/dX is the sulfate concentration gradient in mmol cm^{-1}. 'X' is the depth (cm) from sediment surface, D_s (cm^2 sec^{-1}) is the molecular diffusivity corrected for tortuosity, φ is the average porosity. D_s is calculated from the formula

$$D_s = D_o/1+n (1-\varphi) \qquad \textbf{Eq-3}$$

where D_o= sulfate diffusivity in the absence of particles. Variation in D_o with temperature is calculated using an empirical relation based on data set from Li and Gregory (1974). For the sea bed temperature of 28°C, D_o is 11.0595×10^{-6} cm^2 s^{-1} using n = 3 for clays and silt (Iversen and Jørgensen, 1993). In this study, advective pore water transport (eg. bioirrigation) or reoxidation of sulfide within the sediment have been neglected, since the error in calculation due to this limitation is beyond the scope of the present work.

The relative content of terrestrially derived organic carbon flux is calculated using the mass balance equation:

$$\delta_{TOC} = F_T\delta_T + (1\text{-}F_T)\,\delta_M \qquad \textbf{Eq-4}$$

where δ_{TOC}, δ_T and δ_M are the carbon isotopic compositions of total, terrestrially derived organic and marine phytoplankton organic contents respectively. F_T and $(1\text{-}F_T)$ are the flux of terrestrial and marine phytoplankton derived organic carbon respectively. The values of δ_T = -26‰ and δ_M = -20‰ have been assumed following the studies of Fontugne and Duplessy (1986).

4. Results

4.1 Geophysical and Geological

High resolution shallow seismic profiles (Figures 2A and B) show a wedge shaped sediment package characterized by low amplitude continuous parallel reflectors extending seaward up to a water depth of 50 m. However, the seafloor bathymetry on the wedge is moderately affected due to the crookedness in the seismic Line-5 between the arrow marked locations (fix numbers 138-142). The sediment wedge thickens towards shore and pinches out around 50 m water depth (~24.5 km off the Goa coast). The weak reflectors within the wedge downlap against a planar surface (referred to here as maximum flooding surface, MFS). Overlying the numerous buried channels, a gently inclined wavy surface (referred to here as transgressive surface, TS) can be recognized. A strongly reflecting sediment package (referred to here as transgressive system tract, TST) is sandwiched between the MFS and TS. The channel fill is acoustically transparent and possibly comprised of homogenous fine grained sediments. Figures 2 A and B show acoustic maskings of variable widths on the seismic sections. This masking is caused by the presence of free gas in the sediment. It is characterized by high amplitude, reverse polarity reflection (bright spot) and the masking of the underlying seismic record. The enhanced reflection demarcates the free gas front and lies 1.2 to 5 m below the seabed and is confined to the fine grained sediment wedge. Width of the masking increases with shallowing water depth. Depth to the gas front decreases with decrease in water depth

(Fig. 2A). Acoustic masking beyond 40 m water depth is rarely seen on the seismic sections. The acoustic masking zones show multiple reflections of the gas front.

Average sediment porosities measured using MSCL are 80% for all the sites except at one location Sasu123/7, where it is about 86%. There is no appreciable vertical variation in porosity. The grain size analyses of surface sediments (Fig. 3A) depict dominance of clay (70-91%) and minor sand (0.2-1.6%) content. The vertical distribution at Site Sasu 106/5 and Sasu106/8 show dominance of clay and silt sized fractions compared to sand (Fig. 3B). A sand peak at Site Sasu106/8 is due to ~10 cm thick shell bed.

4.2 Geochemical

The concentrations of various anions (SO_4^{2-}, PO_4^{3-}, NH_4^+ and TA), CH_4, TOC and carbon stable isotope ratios of CH_4, CO_2 and TOC are presented in Table 2. The SO_4^{2-} concentration profiles at Sasu123/1 to Sasu123/11 show linear trends with gradients ranging from 0.042 $mMcm^{-1}$ to 0.288 $mMcm^{-1}$ (Fig. 4). Occasional deviation has been observed in the top sediments. Similar deviation has been reported by Goldhaber and Kaplan (1980) elsewhere who attributed this deviation to sulfide oxidation *in situ* or during sample handling. Depth integrated sulfate reduction rates (J) range from 0.0018 to 0.0126 $mmolcm^2y^{-1}$ (Fig. 5). Only at Sasu123/1 the SO_4^{2-}-CH_4 transition zone (SMTZ) has been demarcated due to a sharp rise in the headspace methane concentration (from 22.9 to 530 ppm). The head space methane concentrations vary from 2 to 20 ppm and gently increase with depth at other sites. The SMTZ at Sasu123/1 occurs around 0.7 m below the seabed. Extrapolated SMTZ at sites Sasu123/3, 4, 7 and 11 occur at 1.88, 2.0, 2.25 and 1.70 m respectively below the seabed.

The total alkalinity (TA) increases from 7.4 to 33.6 mM with depth whereas it varies between 2.6 and 23.8 mM at sites Sasu123/3, 4, 7 and 11. In contrast to this observation, the TA gradient is gentle and increases with depth to a maximum of 9.7 mM at location Sasu123/10.

Increase in PO_4^{3-} and NH_4^+ concentrations with depth have been noted at all sites with variable gradients and fluctuations (Fig. 6). The site Sasu123/1 shows maximum down

core enrichment of both PO_4^{3-} and NH_4^+ concentrations, 124.5 and 2542 μM respectively compared to other sites. In contrast, the maximum PO_4^{3-} and NH_4^+ concentrations recorded at sites Sasu123/3, 4, 7, 11 and 10 vary between 7.5 and 44.2 μM, and 897 and 1686 μM respectively.

The carbon isotopic compositions of TOC, headspace CH_4 and CO_2 are shown in figure-7. The $\delta^{13}C_{TOC}$ varies between -22 and -23‰ (avg: -22.3±0.39). The calculated terrestrial organic carbon flux (F_t %) at sites Sasu123/1, 3, 4 and 10 varies from 31-46%, 26-51%, 31.7-50% and 30-38.3% respectively. The $\delta^{13}C_{CH4}$ data show highly depleted carbon isotopic ratios (as low as -88.9‰) typical of biogenic methane. A Carbon isotopic enrichment of residual methane is observed at all sites. Both $\delta^{13}C_{CO2}$ and $\delta^{13}C_{CH4}$ show nearly parallel trends at sites Sasu123/3, 7 and 11. The $\delta^{13}C_{CO2}$ values tend to approach $\delta^{13}C_{TOC}$ values towards the top of the cores.

The total organic contents (TOC %) vary from 1 to 3.2% (avg: 2.4±0.3%) and the ratio of TOC/ TN from 6.9 to 20.3 (avg: 13.1±2.1). Both TOC% and TOC/TN ratios show significant vertical fluctuations (Fig-8). TOC% and TOC/TN ratios in the surface grab samples varies from 2 to3.1% and 8.6 to 12.1 respectively (Fig. 9).

5. Discussion

5.1 Sedimentation and gas accumulation

The three sequence boundaries proposed by Haq (1991) and Meyers and Milton (1996) [i.e., erosional surface (ES), transgressive surface (TS) and maximum flooding surface (MFS)] are recognized in the high-resolution seismic data acquired off Goa. The undulating erosional surface cutting through late Pleistocene sediments represents an incised fluvial valley (Fig. 2A and Fig. 2B) and may be attributed to emergence of the shelf during the last glacial maxima. The TS marks the post glacial rise of the sea level and represents the initial flooding surface. The transgressive system tract (TST) overlying TS shows strong reflections suggesting a possible sandy nature of the sediment package. TST is overlain by the MFS which marks the time of maximum flooding or transgression

of the shelf and it separates the transgressive and high stand system tracts (Posamantier and Allen, 1999; Catuneanu, 2006).

During the last glacial maxima (~18000yr), sea level fell by ~120 m (Fairbanks, 1989) which resulted in the formation of the ES. The sea level rose from 100 m to 80 m below present level during 14500-12500 years BP at a rate of ~10 m/ ky (Hashimi et al., 1995). Following a still stand of 2500 years, the sea level further rose to the present level at a rate of 20 m/ ky during 10000-7000 years BP. From 7000 year BP to present, minor sea level fluctuations have been recorded (Hashimi et al., 1995). The maximum flooding surface (MFS) might have developed around 7000 years BP. Apparently undisturbed, progradational stacking pattern of weak but continuous reflectors over the MFS resulted in the formation of the fine grained sediment wedge. This fine grained sediment wedge can be traced all along the west coast in water depths between 10 and 50 m (Siddiquie et al., 1981; Karisiddaiah et al., 1993; Karisiddaiah and Veeraya, 1996; Ramprasad et al. 2005).

The acoustic blankings observed in high resolution seismic data suggest that the late Holocene sediment wedge is amenable for accumulation of gas. The observed acoustic masking is attributed to the presence of gas bubbles (predominantly free methane gas) in the sediments. Gas charged sediment attenuates the acoustic energy and limits the sub-bottom penetration thereby masking all underlying stratigraphic features (Hovland and Judd, 1988, Judd and Hovland, 1992; Judd and Hovland, 2007). The high amplitude, reverse polarity seismic reflection results from the impedence contrast produced by the gas bubbles. The enhanced reflections (gas front) lie approximately 1.2 to 5 m below the seabed. Siddiquie et al. (1981) observed 2 to 3 mm size gas bubbles, predominantly methane, at a depth of 3.5 to 4 m below the seabed in sediment cores off Bombay, and estimated gas saturation of ~10% of the volume of the sediment.

We attribute the variation in the depth of the gas front to change in hydrostatic pressure which results in fluctuations of methane solubility (Wever and Fiedler, 1995; Kim et al., 2004; Lee et al., 2005; Wever et al., 2006; Diez et al., 2007b). Above the free gas front, methane resides in a soluble phase in the pore waters due to undersaturation at the ambient temperature and hydrostatic pressure. The maximum extent of the gas front is

observed at the shallowest site (Sasu123/1) (Fig 2A and B) and the width decreases with the increase in water depth in the study area. Hart and Hamilton (1993) and Emeis et al. (2004) observed patchy gas charged zone and widening of acoustic masking landwards as the sediment thickness increases. The grain size distribution data (Fig. 3A) does not show much variation with water depth, and does not support facies control on lateral distribution of gas as reported by Diez et al (2007a) elsewhere. Lower hydrostatic pressure in the shallow waters reduces methane solubility causing increase in volume of free gas in sediment which causes gas bubbles to escape from the sediment (Lee et al., 2005). Although seepage of gas has not been observed within the study area, possibility of its presence in the shallower depths needs further investigation by deploying a high frequency echosounder and divers.

The paleo channels (Fig. 2A and B) are acoustically transparent and possibly filled with homogenous fine grained sediment. These types of incised valley fills (Kindinger et al., 1994; Durán et al., 2007) and buried paleo estuaries (Marlow et al., 1996), lakes and bogs (Gontz et al., 2002; Rogers et al., 2006) and lagoonal sediments are normally rich in organic matter and have been considered as potential shallow methane sources. The scattered distributions of gas saturated zones have also been linked to spatial distribution of such buried gas sources (Weschenfelder et al., 2006). However, from the seismic records, no obvious relation could be discerned with the observed buried channels and gas masking. The gas masking which often look like gas chimneys is apparently controlled by gas built up within the sediment wedge and subsequent masking of underlying features. Analyses of more seismic lines are required for further confirmation.

5.2 Sediment Geochemistry

Geochemical profiles of sediment pore fluids in the cores from the study area show variation with water depth. Concentration profiles of sulfate, methane, alkalinity, ammonium and phosphate at sites Sasu123/3, 4, 7 and 11 are transitional between the two sites, Sasu123/1 and 10. Depth integrated sulfate reduction rates (J) decrease with increasing water depth and decreasing sediment wedge thickness (Fig. 5). The biological sulfate reduction (Harrison and Thode, 1958; Canfield, 2001; Megonigal et al. 2003;

Canfield et al., 2005) is a bacterially-mediated metabolic process which results in the breakdown of S-O bonds of dissolved sulfate, and subsequent production of H_2S gas. Organoclastic degradation (Froelich et al., 1979) and anaerobic methane oxidation (AMO) are the two pathways of sulfate reduction represented by equations 5 and 6:

$(CH_2O)_{106}(NH_3)_{16}(H_3PO_4) + 53\ SO_4^{2-} \rightarrow 106\ HCO_3^- + 53\ HS^- + 16\ NH_3 + H_3PO_4 + 53\ H^-$ **Eq-5**

$CH_4 + SO_4^2 \rightarrow HCO_3^- + HS^- + H_2O$ **Eq-6**

AM AMO is attributed to consortium of CH_4-oxidizing archaea and sulfate-reducing bacteria (Hinrichs et al., 1999; Boetius et al., 2000; Orphan et al., 2001). Methane and sulfate consumptions by AMO give rise to the sulfate methane transition zone (SMTZ). AMO is also responsible for high alkalinity due to production of bicarbonate (HCO_3^-) and hydrogen sulfide (HS^-). The inferred shallower SMTZ (~0.7 m below seabed) and high alkalinity at Sasu123/1 is attributed to high methane flux and AMO. The extrapolated depth to SMTZ at sites Sasu123/3, 4, 7 and 11 varies between 1.7 and 2.25 m below the seabed. The high methane flux at Sasu123/1 may be linked to higher flux of reactive organic matter (Canfield, 1994; Martens et al., 1998). This resulted in rapid depletion of dissolved pore water sulfate in the vicinity of the sediment-water interface and increase in methane concentration due to availability of suitable substrates. In the marine sediments, bacterial carbonate reduction is the dominant methanogenic pathway since other methanogenic substrate like acetate is depleted due to organoclastic sulfate reduction (Whiticar and Faber, 1986, Whiticar, 1999; Whiticar, 2002). Equations 7 and 8 represent the carbonate reduction and acetate fermentation pathways respectively.

$CO_2 + 8H^+ + 8e^- \rightarrow CH_4 + 2H_2O$ **Eq-7**

$CH_3COOH \rightarrow CH_4 + CO_2$ **Eq-8**

Highly depleted carbon isotopic ratios of methane in all the cores (Fig. 7) strongly advocate the microbial origin of methane through carbonate reduction pathways as suggested by Whiticar and Faber (1986) and Whiticar (1999). A $\Delta\delta_{CO2\text{-}CH4}$ of 59-63‰ at Sasu123/1 also indicates carbonate reduction pathway (Gallimov, 2006). However, the contribution of acetate fermentation in methanogenesis is rather difficult to assess in the absence of $\delta D_{CH4,}$ $\delta^{13}C_{acetate,}$ and acetate concentration measurements as indicated by Conrad (2005). Carbon isotopic enrichment in the residual methane towards the top of the

cores (Fig. 7) is attributed to kinetic isotope effect which involves preferential consumption of ^{12}C-CH_4 via anaerobic oxidation of methane (Alperin et al., 1988; Whiticar, 1999). The carbon isotope separation ($\Delta\delta_{CO2\text{-}CH4}$) between residual methane and CO_2 decreases towards the top of the cores. This is attributed to decrease in CO_2 contribution from methane oxidation and increasing contribution of organiclastic derived CO_2 which approaches $\delta^{13}C_{TOC}$.

The pore-water ammonium and phosphate concentrations at Sasu123/1 are comparatively much higher than at other sites, which suggest greater abundance of reactive (labile) organic matter at Sasu123/1. Minimum ammonium concentrations were encountered at location Sasu123/10. Ammonium and phosphate are produced via bacterial decomposition of organic compounds (eq. 5). The oscillations/variations in the phosphate and ammonium concentration profiles may be due to the reoxidation (ANAMOX: Dalsgaard and Thamdrup, 2002) and adsorption-desorption reactions with solid phases viz., clay, organic particulates and Fe-oxyhydroxides (Krom and Burner, 1980; Boatman and Murray, 1982; Sundby et al., 1992; Morse and Morin, 2005).

Although fluid chemistry i.e., sulfate reduction, methanogenesis, ammonium and phosphate concentrations unequivocally suggest greater availability of reactive organic compounds at Sasu123/1 location, no significant variation in TOC content from shallowest to deepest cores is observed. Higher availability of reactive organic component for bacterially mediated reactions requires preservation of these compounds from oxidative decomposition during sedimentation (Hedges and Keil, 1995; Hartnett et al., 1998; Hedges et al., 1999; Suthhof et al. 2000; Gélinas et al., 2001). Apparently enhanced preservation of labile organic compounds in the shallow water is attributed to limited transportation of organic load and higher sedimentation rate (Canfield, 1991; Iversen and Jørgensen, 1993; Canfield, 1994).

6. Conclusions

In this work we report occurrences of shallow gas off the coast of Goa, west coast of India. Seismic studies show that the gas pockets are located within a fine grained sediment wedge which pinches out offshore at a water depth of ~50 m. In the gas charged

sediments, the gas front (characterized by enhanced reflections) lies 1.2 to 5 m below the seabed. Acoustic masking zones are widest near shore (<15 m), and rarely seen beyond the water depth >40 m. We also have observed a shallowing of the gas front towards the shore. The observed and extrapolated SMTZ lies between 0.7 and 2.25 m below the seabed in the gas charged sites. Microbial methane is the most dominant gas below SMTZ, and creates a bubble phase at concentrations higher than saturation at the ambient P-T conditions. The bubble phase is indicated by enhanced reflection on the seismic records. Higher concentrations of pore-water methane, phosphate and ammonium in the shallowest core site (Sasu123/1) compared to all other sites suggests preferential availability of reactive organic compounds for microbially mediated biodegradation processes. We attribute the higher availability of labile organic compounds in shallow near shore sediments to relatively low oxidative decomposition owing to relatively high sedimentation rate and less horizontal transportation. We could not find conclusive evidence of methane contribution from the buried channels or deeper late Pleistocene sediments. However, such a possibility can not be ruled out. Perhaps long cores penetrating through the buried channels would throw more light on this problem. Since shallow gases occur all along the west coast of India within a restricted depth zone, more work is required on their distribution and genesis to assess its environmental/ engineering impact and influence on biological community. The present work has demonstrated that the biogeochemical processes in Holocene organic rich sediments are responsible for the accumulation of gases which results in seismic blanking of underlying stratigraphy as observed in many gas charged sediments globally. In view of this, patchy distribution of gas blanking/ curtains and its link with deep seated gas sources need to be revisited.

Acknowledgements

We thank the Director of NIO Dr. Satish Shetye for providing facilities to publish this work. We thank Dr. Ana García-García, an anonymous reviewer and the editor John T. Wells for their careful reviews and comments.

Reference

Alperin, M.J., Reeburgh, W.S., Whiticar, M.J., 1988. Carbon and hydrogen isotope fractionation resulting from anaerobic methane oxidation. Global Biogeochem. Cycles 2, 279-288.

Berner, R.A., 1980. Early Diagenesis: A Theoretical Approach. Princeton University Press, 241pp.

Boatman, C.D., Murray, J.W., 1982. Modeling exchangeable NH_4^+ adsorption in marine sediments: process and controls of adsorption. Limnol. Oceanogr. 27, 99– 110.

Boetius, A., Ravenschlag, K., Schubert, C.J., Rickert, D., Widdel, F., Giesecke, A., Amann, R., Jørgensen, B.B., Witte, U. and Pfannkuche, O., 2000. A marine microbial consortium apparently mediating anaerobic oxidation of methane. Nature 407**,** 623–626.

Boudreau, B.P., Algar, C., Johnson, B.D., Croudace, I., Reed, A., Furukawa, Y., Dorgan, K.M., Jumars, P.A., and Grader, A.S., 2005. Bubble growth and rise in soft sediments. Geology 33, 517-520.

Canfield, D.E., 1989. Sulfate reduction and oxic respiration in marine sediments: implications from organic carbon preservation in euxinic environments. Deep Sea Res. 36, 121-138.

Canfield, D.E., 1991. Sulfate reduction in deep sea sediments: Amer. J. Sci. 291, 177-188.

Canfield, D.E., 1994. Factors influencing organic carbon preservation in marine sediments. Chem.Geol. 114**,** 315-329.

Canfield, D. E., 2001. Biogeochemistry of sulfur isotopes. Rev. Mineral. Geochem. 43, 607-636.

Canfield, D.E., Kristensen E., Thamdrup B., 2005. Aquatic Geomicrobiology. Advances in marine biology 48, 638 pp.

Catuneanu, O., 2006. Principles of sequence stratigraphy, Elsevier. 375 pp.

Conrad, R., 2005. Quantification of methanogenesis pathways using stable carbon isotope signatures: a review and a proposal. Org. Geochem. 36, 739-752.

Dalsgaard, T., Thamdrup, Bo., 2002. Factors controlling anaerobic ammonium oxidation with nitrite in marine sediments. Appl. Environ. Microbiol. 8, 3802-3808.

Diez, R., García-Gil, S., Durán, R., Vilas, F., 2007a. Gas accumulations and their association with particle size distribution patterns in the Ŕia de Arousa seabed ,Galicia, NW Spain: an application of discriminant analysis. Geo-Mar. Lett. 27, 89-102.

Diez,, R., García-Gil, S., Durán, R., Vilas, F., 2007b. Gas-charged sediments in the Ŕia de Arousa: Short- to long term fluctuations. Estuar. Coast. Shelf Sci. 71, 467-479.

Duan, Z.H., Mao, S.D., 2006. A thermodynamic model for calculating methane solubility, density and gas phase composition of methane-bearing aqueous fluids from 273 to 523 K and from 1 to 2000 bar. Geochim. Cosmochim. Acta**.** 70, 3369-3386.

Durán, R., García-Gil, S., Diez, R. and Vilas, F., 2007. Stratigraphic framework of gas accumulations in the Ría de Pontevedra (NW Spain). Geo-Mari.Lett. 27, 77-88.

Emeis, K.C., Brüchert, V., Currie, B., Endler, R., Ferdelman, T., Kiessling, A., Leipe, T., Noli-Peard, K., Struck, U., Vogt, T., 2004. Shallow gas in shelf sediments of the Namibian coastal upwelling ecosystem. Cont. Shelf Res. 24, 627–642.

Fairbanks, R.G., 1989. A 17,000 year glacio-eustatic sea level record: influence of glacial melting rates on the Younger Dryas: influence event and deep-ocean circulation. Nature 342, 637-642.

Fleischer, P., Orsi, T.H., Richardson, M.D., Anderson, A.L., 2001. Distribution of free gas in marine sediments: a global overview. Geo-Mar. Lett. 21, 103-122.

Floodgate, G.D., Judd, A.G., 1992. The origins of shallow gas. Cont. Shelf Res.10, 1145-1156.

Fontugne, M. R., Duplessy, J-C., 1986. Variations of the monsoon regime during the upper quaternary: Evidence from carbon isotopic record of organic matter in north Indian ocean sediment core. Palaeo. Palaeo. Palaeo. 56, 69-88.

Froelich, P.N., Klinkhammer, G.P., Bender, M.L., Luedtke, N. A., Heath, G. R., Cullen, D., Dauphin, P., Hammond, D., Hartman, B.,Maynard, V., 1979. Early oxidation of organic matter in pelagic sediments of the eastern equatorial Atlantic: suboxic diagenesis. Geochim. Cosmochim. Acta 43, 1075–1090

Gallimov, E.M., 2006. Isotope organic geochemistry. Org. Geochem. 37, 1200-1262.

García-García, A., García-Gil, S., Vilas, F., 2005. Quaternary evolution of the Ría de Vigo, Spain. Mar.Geol. 220,153–179.

García-García, A., Tesi, T., Orange, D., Lorenson, S., Langone, L., Herbert, I., Dougherty, J., 2007. Understanding shallow gas occurrences in the Gulf of Lions. Geo-Mar. Lett. 27, 143-154.

Gélinas, Y., Baldock, J.A., Hedges, J.I., 2001. Organic carbon composition of marine sediments: effects of oxygen exposure on oil generation potential. Nature 294, 145-148.

Gieskes, J.M. Gamo, T., Brumsack, H., 1991. Chemical methods for interstitial water analysis aboard JOIDES Resolution. Oceanon Drilling Program, Texas A&M university. Technical Note 15, 60pp.

Gontz, A.M., Belknap, D.F., Kelley, J.T., 2002. Seafloor features and characteristics of the Black Kedges Area, Penobscot Bay, Maine, USA. J. Coast. Res.36, 333–339.

Goldhaber, M.B., Kaplan, I.R., 1980. Mechanisms of sulfur incorporation and isotope fractionation during early diagenesis in sediments of the Gulf of California. Mar.Chem. 9, pp. 95–143.

Haq, B.U., 1991. Sequence stratigraphy, sea-level change and significance for the deep sea. In: Macdonal, D.I.M (Ed.), Sedimentation, Tectonics and Eustasy: Sea-Level Changes at Active Margins. Spec. Pub. Int. Assoc. Sed., 12, 3-39.

Harrison, A.G., Thode, H.G., 1958. Mechanism of the bacterial reduction of sulphate from isotopic fractionation studies. Faraday Soc. Transac. 54, 84-92.

Hashimi, N.H., Nigam, R., Nair, R.R., Rajagopalan, G., 1995. Holocene sea level fluctuations on western Indian continental margins: An update. J. Geol. Soc. India 46, 157-162.

Hart, B.S., Hamilton, T.S., 1993. High resolution acoustic mapping of shallow gas in unconsolidated sediments beneath the strait of Georgia, British Columbia. Geo-Mar. Lett.13, 49-55.

Hartnett, H.E., Keil, R.G., Hedges, J.L., Devol, A.H.,1998. Influence of oxygen exposure time on organic carbon preservation in continental margin sediments. Nature 391, 572-574.

Hedges, J.I., Hu, F.S, Devol, A.H., Hartnett, H.E., Tsamakis, E., Keil, R.G., 1999. Sedimentary organic matter preservation: a test for selective degradation under oxic conditions. Amer. J. Sci. 299, 529–555

Hedges, J.I. and Keil, R.G., 1995. Sedimentary organic matter preservation: an assessment and speculative synthesis. Mar. Chem. 49, 81-115.

Hinrichs, K.U., Hayes, J.M., Sylva, S.P., Brewer, P.G., DeLong, E.F., 1999. Methane-consuming archaebacteria in marine sediments. Nature 398, 802-805.

Hobbs, C.H., 2004. Geological history of Chesapeake Bay, USA. Quarter. Sci. Rev. 23, 641–661.

Hovland, M., Judd, A.G., 1988. Seebed pockmarks and seepages: impact on geology, biology and the marine environment. Graham and Trotman, London. 293 pp

Hovland, M., Judd, A.G., 1992. The global production of methane from shallow submarine sources. Cont. Shelf Res.12, 1231-1238.

Iglesias, J., García-Gil, S., 2007. High resolution mapping of shallow gas accumulations and gas seeps in San Simón Bay (Ría de Vigo, NW Spain). Some quantitative data. Geo-Mar.Lett. 27, 103-114.

Iversen, N. and Jørgensen, B. B. 1993. Diffusion coefficients of sulfate and methane in marine sediments: Influence of porosity. Geochim. Cosmochim. Acta 57, 571–578

Judd, A.G., Hovland, M., 1992. The evidence of shallow gas in marine sediments. Cont. Shelf Res.10, 1081-1095.

Judd, A.G., 2003. The global importance and context of methane escape from seabed. Geo-mar. Lett. 23, 147-154.

Judd, A.G., Hovland, M., 2007. Seabed Fluid Flow, Cambridge. 475 pp.

Karisiddaiah, S.M., Subba, R.L.V., 2002. Scenario of gas-charged sediments and gas hydrates in the western continental marigin of India. J. Geophysic. 23, 33-41.

Karisiddaiah, S.M., Veerayya, M., 1996. Potential distribution of subsurface methane in the sediments of the eastern Arabian Sea and its possible implications. J. Geophysic. Res. 101, 25887-25895.

Karisiddahia, S.M., Veerayya, M., Vora, K.H., 2002. Seismic and sequence stratigraphy of central western continental marigin of India: late-Quaternary evolution. Mar. Geol. 192, 335-353.

Karisiddahia, S.M., Veerayya, M., Vora, K.H., Wagle, B.G., 1993. Gas-charged sediments on the inner continental shelf off western India. Mar. Geol.110, 143-152.

Kim, D.C., Lee, G.H., Seo, Y.K., Kim, G.Y., Kim, S.Y., Kim, J.C., Park, S.C., Wilkens, R.H., 2004. Distribution and acoustic characteristics of shallow gas in the Korea Strait shelf mud off SE Korea. Mar. Georesourc. Geotech. 22, 21–31.

Kindinger, J.L., Balson P.S., Flocks J.G., 1994. Stratigraphy of the Mississippi–Alabama Shelf and the Mobile River incised-valley system: origin and sedimentary sequences. SEPM Special Publication 51, 83–95.

Krom, M.D., Berner, R.A., 1980. Adsorption of Phosphate in Anoxic Marine Sediments. Limnol. Oceanogr. 25, 797-806.

Laier, T., Jensen, J.B., 2007. Shallow gas depth-contour map of the Skagerrak-western Baltic Sea region. Geo-Mar. Lett. 27, 127-141.

Lashof, D.A., Ahuja, D.R., 1990. Relative contributions of greenhouse gas emissions to global warming. Nature 344, 529-531.

Lee, G.H., Kim, D.C., Kim, H.J., Jou, H., Lee, Y.J., 2005. Shallow gas in the central part of Korea strait shelf mud off the southeastern coast of Korea. Cont. Shelf Res. 25, 2036-2052.

Li, Y-H., Gregory, S., 1974. Diffusion of ions in sea water and in deep sea sediments. Geochim. Cosmochim. Acta 38, 703-714

Liu, J.P, Milliman, J.D., Gao, S., Cheng, P., 2004. Holocene development of the Yellow River's subaqueous delta, North Yellow Sea. Mar. Geol. 209, 45–67

Marlow, M.S., Hart, P.E., Carlson, P.R., Childs, J.R, Mann, D.M, Anima, R.J., Kayen, R.E., 1996. Misinterpretation of lateral acoustic variations on high-resolution seismic reflection profiles as fault offsets of Holocene bay mud beneath the southern part of San Francisco, Bay California. Mar.Petrol.Geol.13, 341–348.

Martens, C.S., Albert, D.B., Alperin, M.J., 1998. Biogeochemical processes controlling methane is gassy coastal sediments-Part1. A model coupling organic matter flux to gas production, oxidation and transport. Cont. Shelf Res.18, 1741-1770.

Megonigal, J.P., Hines, M.E. and Visscher, P.T., 2003. Anaerobic Metabolism: Linkages to Trace Gases and Aerobic Processes. In: Holland, H.D. and Turekian, K.K. (Eds.), Treatise on Geochemistry, Vol. 8, Biogeochemistry. Elsevier Pergamon. pp. 317-424.

Meyers, K.J., Milton, N.J., 1996. Concepts and principles of sequence stratigraphy. In Emery, D., Meyers, K.J. (Eds.), Sequence Stratigraphy. Blackwel Science, London, 296 pp.

Missiaen, T., Murphy, S., Loncke, L., Heriet. J.P., 2002. Very high-resolution seismic mapping of shallow gas in the Belgian coastal zone. Cont. Shelf Res. 22, 2291-2301.

Morse, W.J., Morin, J., 2005. Ammonium interaction with coastal marine sediments: influence of redox conditions on *K**. Mar. Chem. 95, 107-112.

Nair, R.R., Pylee, A., 1968. Size distribution and carbonate contents of the sediments of the western shelf of India. Bull. National Inst. Sci. India 38, 411-420.

Nair, R.R., Hashimi, N.H., Kidwai, R.M., Guptha, M.V.S., Paropkari, A.L., Ambre, N. V., Muralinath, A.S., Mascarenhas, A., D'Costa, G.P., 1978. Topography and sediments of western continental shelf of India-Vengurla to Mangalore. Indian J. Mar. Sci. 7, 224-230

Nakicenovic, N., 2002. Methane as an energy source for the 21st century. International J. Global Energy Issues 18, 6-22.

Orphan, V.J., House, C.H., Hinrichs, K-U., McKeegan, K.D., DeLong, E.F., 2001 Methane-consuming archaea revealed by directly coupled isotopic and phylogenetic analysis. Science 293, 484– 487.

Posamentier, H.W., Allen, G.P., 1999. Siliciclastic sequence stratigraphy: concepts and applications. SEPM Concepts in Sedimentology and Paleontology 7, pp.210.

Ramprasad, T., Ramana, M.V., Dewangan, P., Anand Dev Paul, K. and Desa, M., 2005., High resolution sparker studies along the inner shelf of Cabo-de-Rama, central west coast of India. 42nd Annual Convention and meeting on Earth System processes related to Earth quakes, Tsunamies and volcanic eruption", Bhopal, India.

Rao, B.R., Veeraya, M., 2000. Influence of marginal highs on the accumulation of organic carbon along the continental slop off western India. Deep-Sea Res. II 47, 303-327.

Rao, P.C., Wagle, B.G. 1997. Geomorphology and surficial geology of the western continental shelf and slope of India: A review. Current Science 73, 330-350.

Reeburgh, W.S., 2007. Oceanic methane biogeochemistry. Chem. Rev. 107, 486-513.

Robb, G.B.N, Leighton, T.G., Dix., J.K., Best, A.I., Humprey, V.F., White, P.R., 2006. Measuring bubble populations in gassy marine sediments: A review. Proceedings of the Institute of Acoustics 28, 60-68.

Rogers, J.N., Kelley, J.T., Belkmap, D.F., Gontz, A., Barnhardt, W.A., 2006. Shallow-water pockmark formation in temperate estuaries: a consideration to origins in the western Gulf of Maine with special focus on Belfast Bay. Mar. Geol. 225, 45–62.

Siddiquie, H.N., Rao, D.G., Vora, K.H. and Topgi, R.S., 1981. Accoustic masking in sediments due to gases on the western continental shelf of India. Mar. Geol. 39, 27-37.

Sills, G.C., Wheeler, S. J., 1992. The significance of gas for offshore operations. Cont. Shelf Res.10, 1239-1250.

Sundby, B., Gobeil, C., Silverberg, N., Mucci, A., 1992. The phosphorous cycle in coastal marine sediments. Limnol. Oceanogr. 37, 1129-1145.

Suthhof, A. Jennerjahn, T.C. Schafer, P and Ittekot, V., 2000. Nature of organic matter in surface sediments from the Pakistan continental margin and the deep Arabian Sea: amino acids. Deep Sea Res. II 47, 329-351.

Taylor, D.I., 1992. Nearshore shallow gas around the U.K. coast. Cont. Shelf Res.10, 1135-1144.

Tucker, M., 1988. Techniques in Sedimentology. Blackwell Scientific Inc. 408 pp.

Vogt, P.R., Halka, J.P, Hagen, R.A., Cronin, T., 2000. Geophysical environment in Chesapeake Bay: Marion–Dufresne sites MD99-2205 2206 and 2208. US Geol Surv Open-File Rep 00-306.

Wagle, B.G., Vora, K.H., Karisiddaiah, S.M., Veerayya, M., Almeida, F., 1994. Holocene submarine terraces on the western continental shelf of India: implications for sea-level changes. Mar. Geol.117, 207-225.

Wever, Th.F., Fiedler, H., 1995. Variability in acoustic turbidity in Eckernförde Bay (SW Baltic Sea) related to annual temperature cycle. Mar. Geol.125, 21-27.

Wever, Th.F., Luhder, R., Voβ, L.H., Knispel, U., 2006. Potential environmental control of free shallow gas in the seafloor of Eckernförde Bay, Germany. Mar. Geol. 225, 1-4.

Weschenfelder, J., Corrêa, I.C.S., Aliotta, S., Pereira, C.M. and De Vasconcellos, V.E. B., 2006. Shallow gas accumulation in sediments of the patos lagoon, southern Brazil anais da academia brasileira de ciências 78, 607-614.

Whiticar, M.J., 1999. Carbon and hydrogen isotope systematics of bacterial formation and oxidation of methane. Chem. Geol. 161, 291-314.

Whiticar, M.J., 2002. Diagenetic relationships of methanogenesis, nutrients, acoustic turbidity, pockmarks and freshwater seepages in Eckernförde Bay. Mar. Geol.182, 29-53.

Whiticar, M.J., Faber, E., 1986. Methane oxidation in sediment and water column environments -Isotope evidence. Org. Geochem.10, 759-768.

Wilkens, R.H., Richardson, M.D., 1998. The influence of gas bubbles on sediment acoustic properties: in situ, laboratory, and theoretical results from Ecernförde Bay, Baltic Sea. Cont. Shelf Res.18, 1859-1892.

Yamamoto, S., Alcauskas, J.B., Crozier, T.E., 1976. Solubility of methane in distilled water and seawater. J. Chem. Engineer. Data 21, 78-80.

Yuan, F., Bennell, J.D., Davis, A.M., 1992. Acoustic and physical characteristics of gassy sediments in the western Irish Sea. Cont. Shelf Res.12, 1121-1134.

Figure and Table captions

1. Map showing coring stations and seismic survey lines and distribution of surface samples collected off Goa, west coast, and India. Isobaths are in meter.
2. **(a)** Seismic profile showing sequence boundaries and gas masking along the survey line-05 and **(b)** line-03. MFS = maximum flooding surface, ES = erosional surface, TS = transgressive surface, TST= transgressive system tract.
3. **(a)** Grain size distribution pattern (wt %) in the surface sediments with water depth. **(b)** Vertical variation in grain size distribution in gravity cores Sasu106/5 and Sasu106/8 located at 16.3 and 29 m water depths respectively.
4. Vertical profiles of pore water total alkalinity, sulfate and methane concentrations in the sediment cores. Dash-dot line indicates the location of the sulfate methane interface (SMTZ).
5. Variation in depth integrated sulfate reduction rates (J) with water depth.
6. Vertical profiles of pore water phosphate and ammonium in the sediment cores.
7. Vertical profiles of $\delta^{13}C_{TOC}$, $\delta^{13}C_{CH4}$ and $\delta^{13}C_{CO2}$ in the sediment cores. Carbon isotope ratios are in permil (‰) relative to VPDB.
8. Vertical profiles of TOC and TOC/TN in the sediment cores.
9. Variations in TOC% and TOC/TN ratios in surface sediments.

Table Captions

1. Locations and water depths of Sasu 123 and Sasu 106 cores.
2. Pore fluid compositions, total organic carbon contents, TOC/ TN ratios and carbon stable isotopic compositions of gases and TOC in the sediment cores. Carbon isotope ratios are in permil (‰) relative to VPDB.

Figure

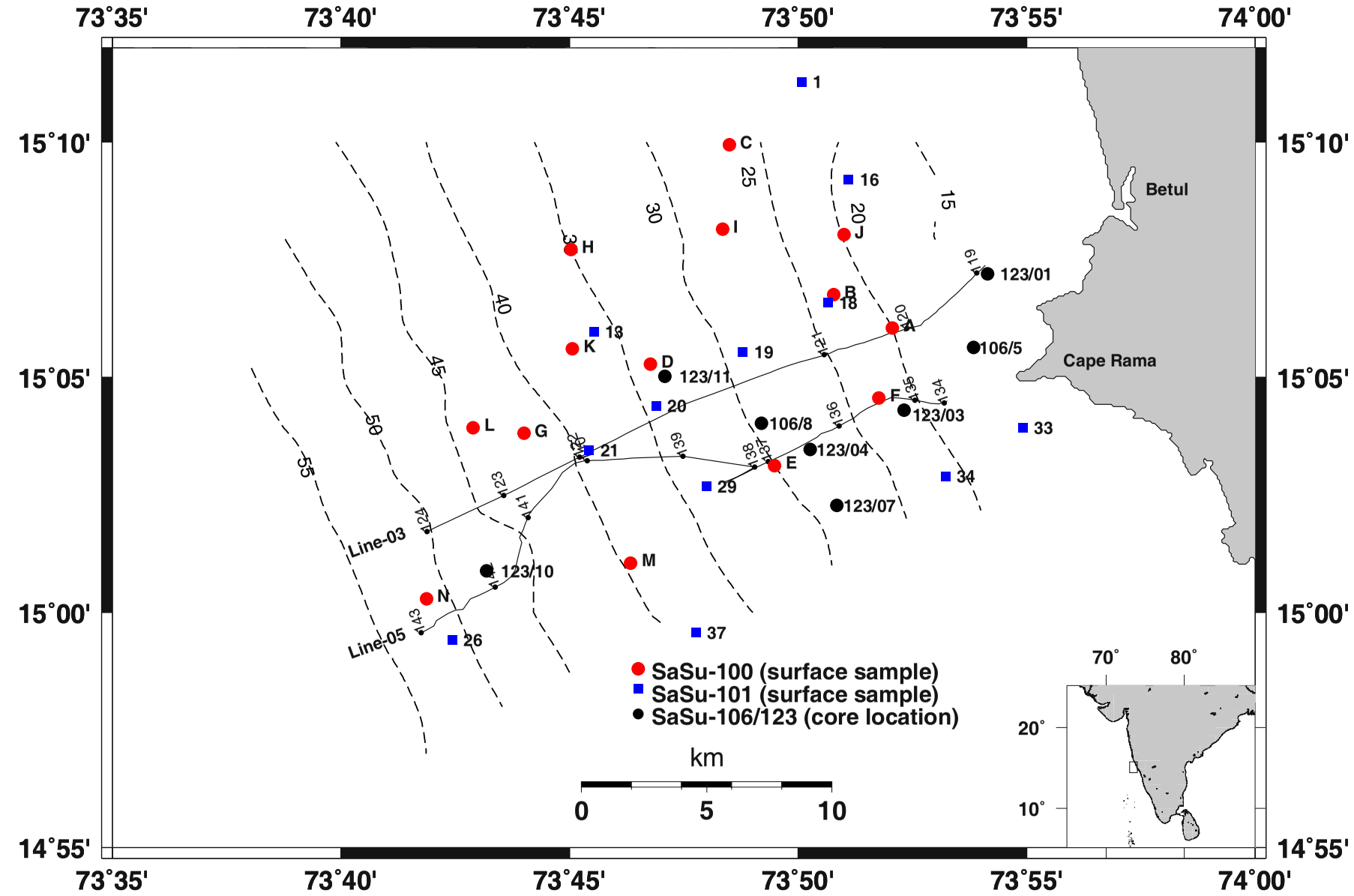
73°35'
73°40'
73°45'
73°50'
73°55'
74°00'
15°10'
15°05'
15°00'
14°55'
Betul
Cape Rama
1
C
16
I
J
H
123/01
B
18
A
106/5
K
18
19
D
123/11
20
F
123/03
L
G
106/8
21
123/04
E
33
29
34
123/07
Line-03
M
123/10
N
Line-05
26
37
SaSu-100 (surface sample)
SaSu-101 (surface sample)
SaSu-106/123 (core location)
km
0
5
10
70°
80°
20°
10°

Figure

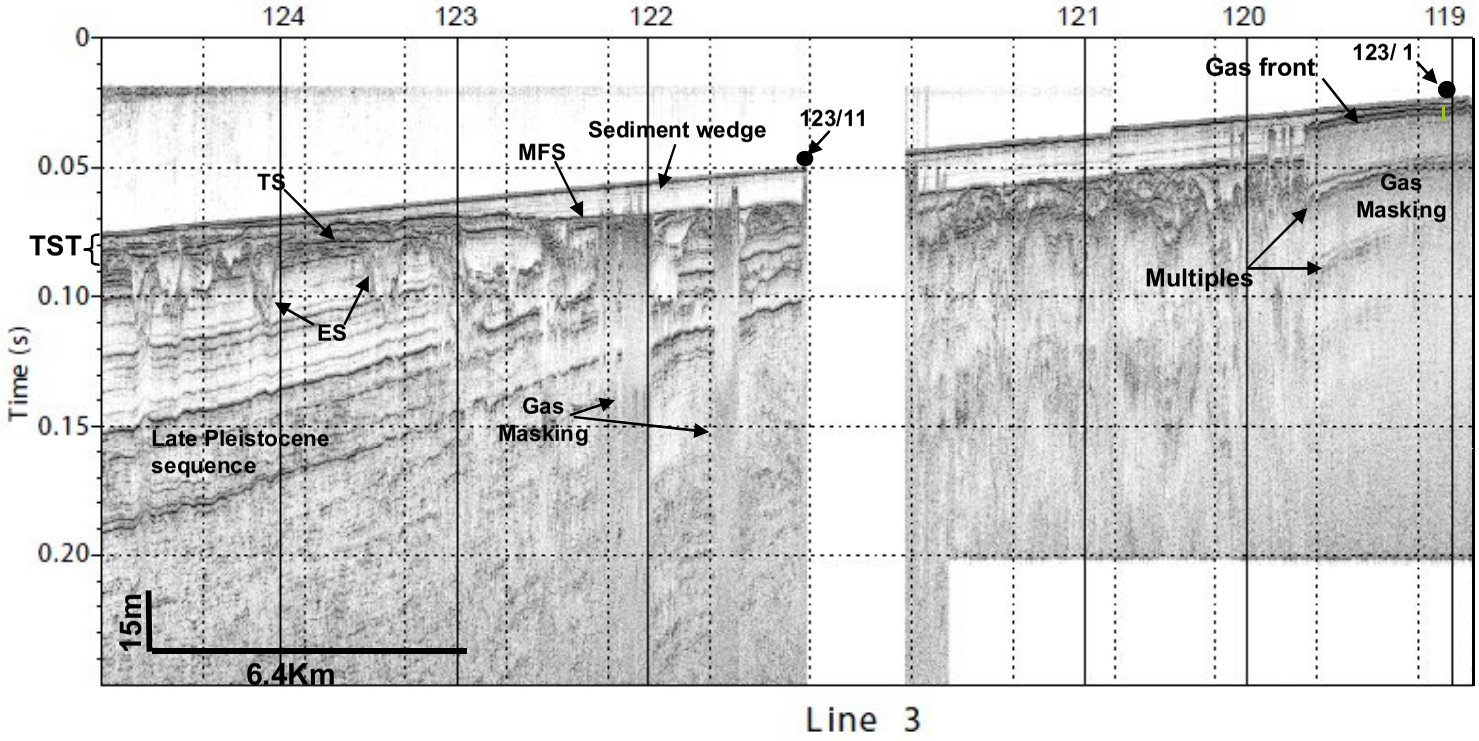

Figure 2A

Figure

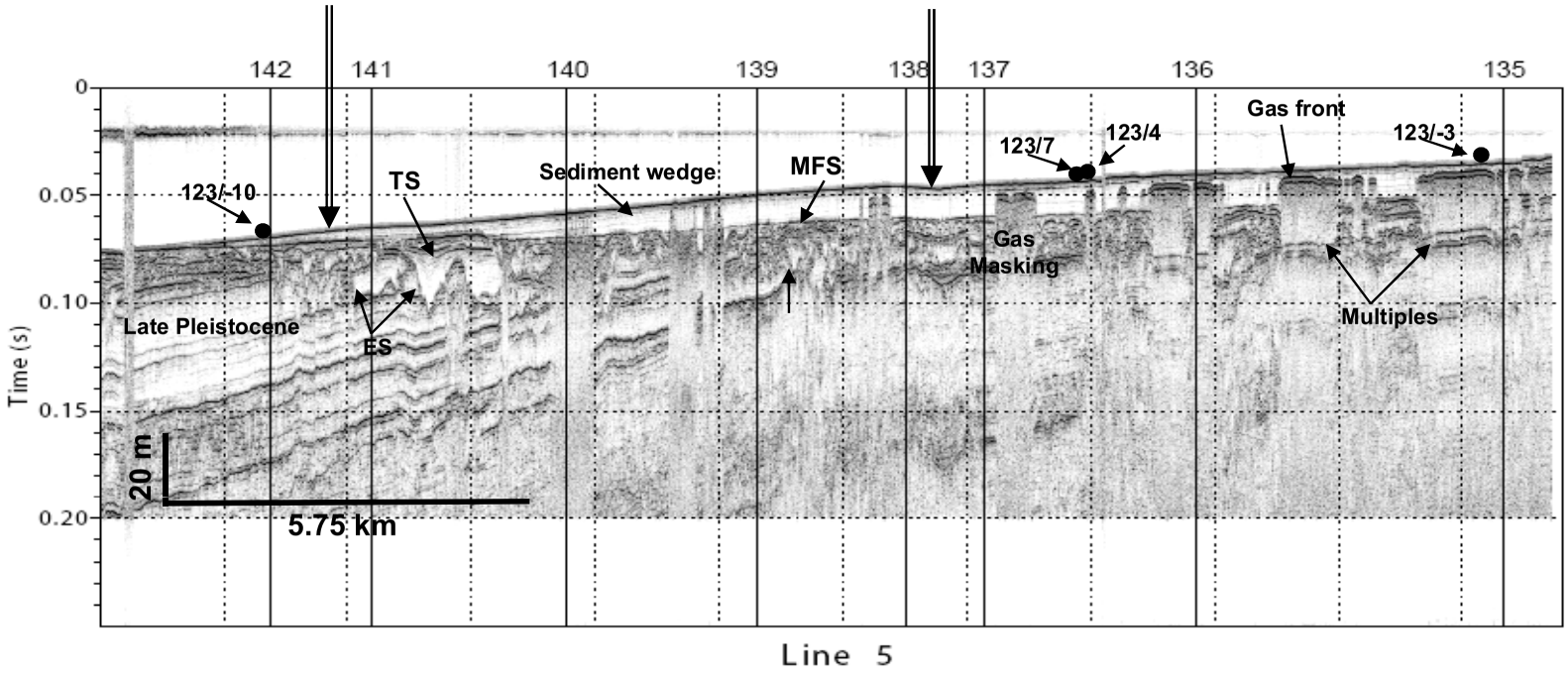

Figure 2 B

Figure

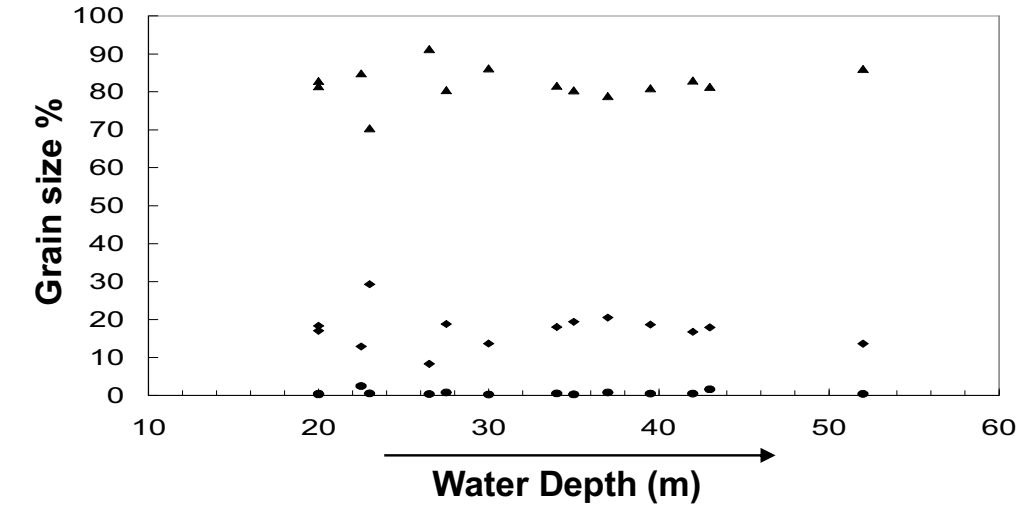

A

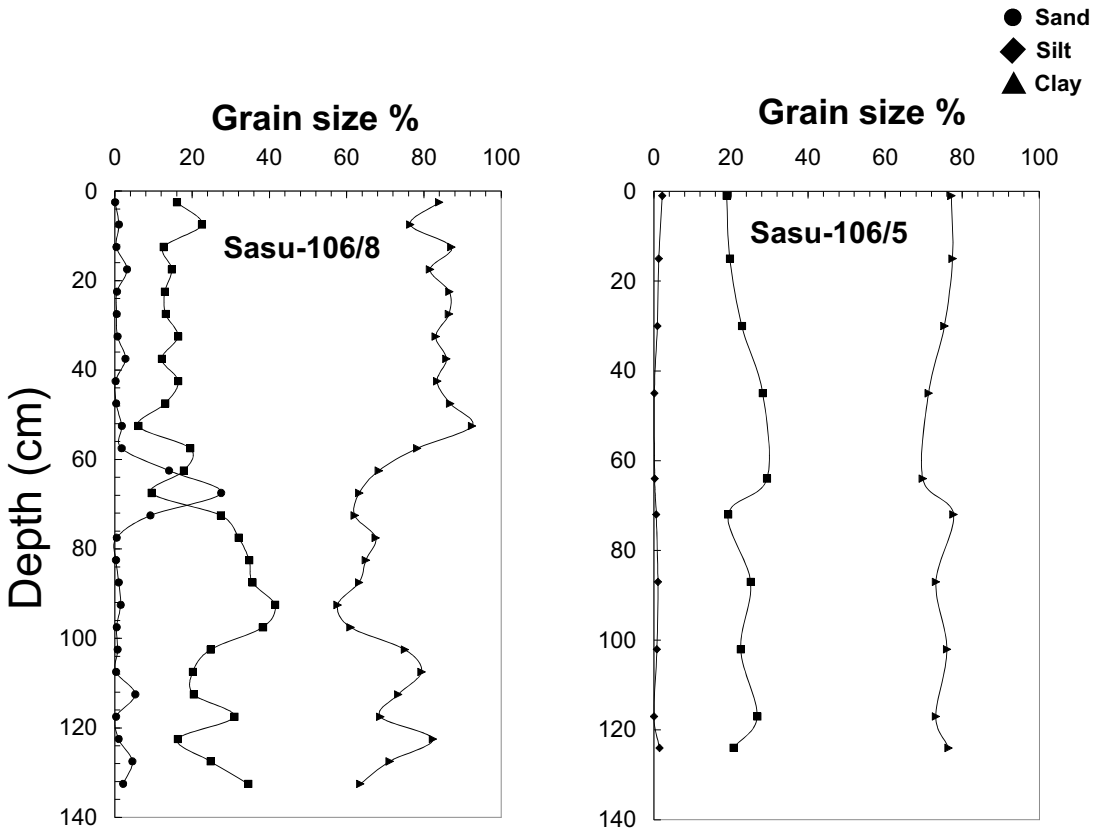

B

Figure-3

Figure

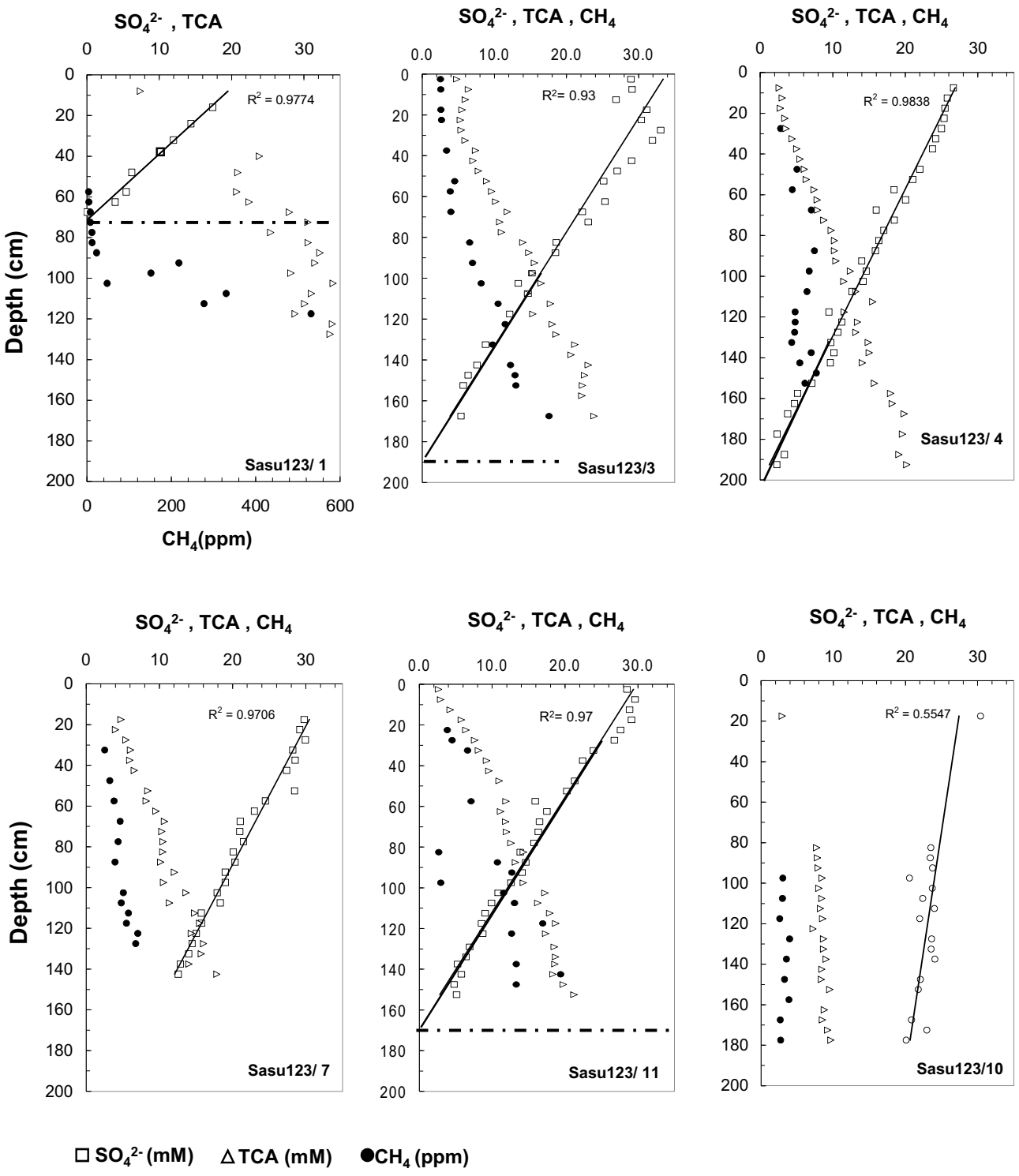

Figure-4

Figure

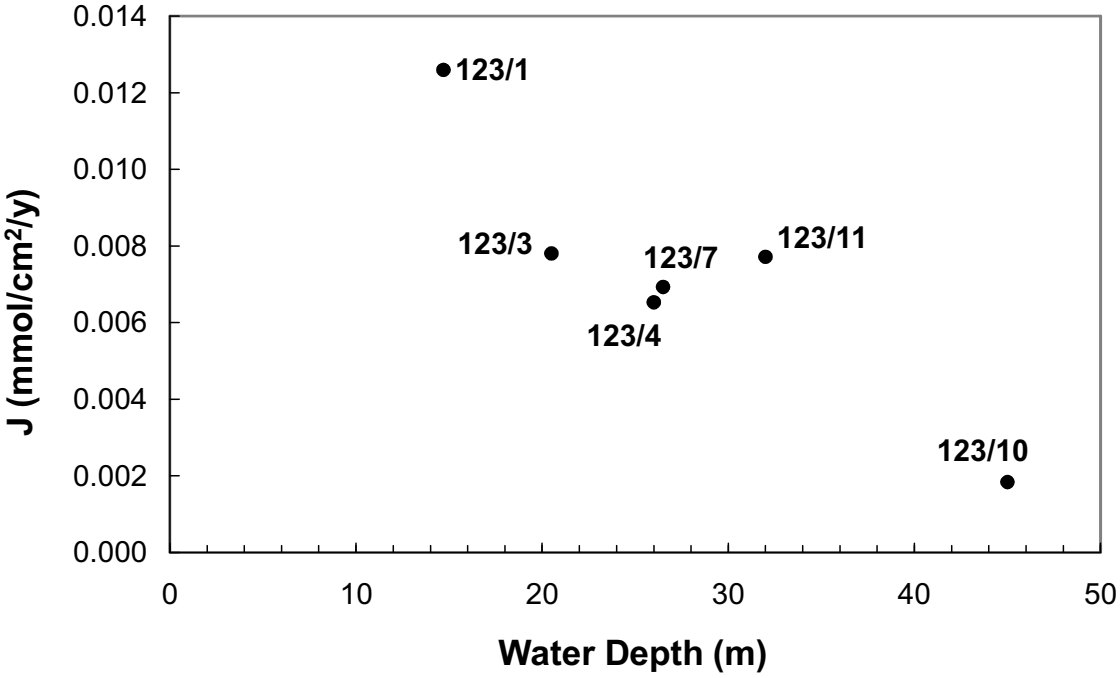

Figure-5

Figure

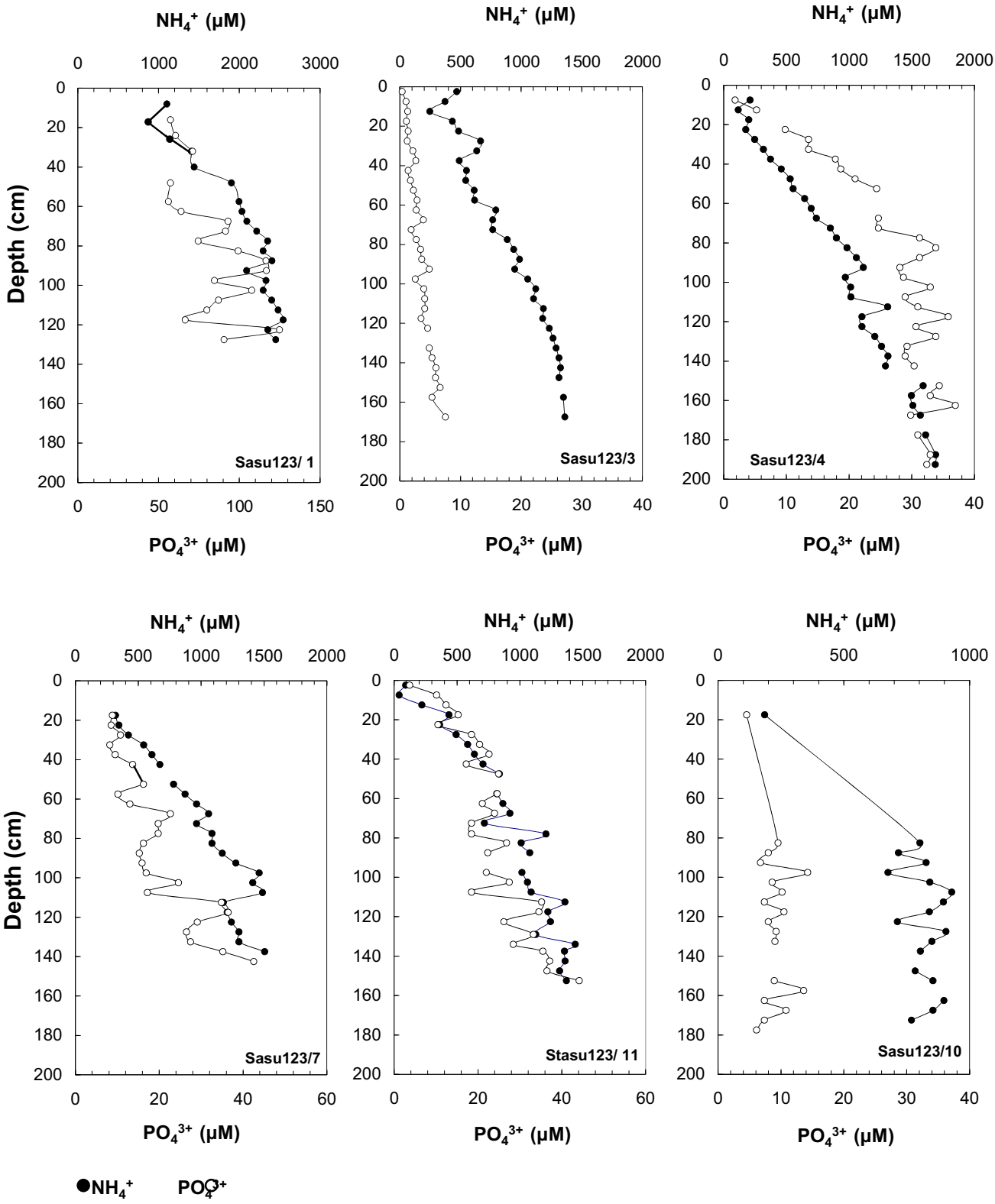

Figure-6

Figure

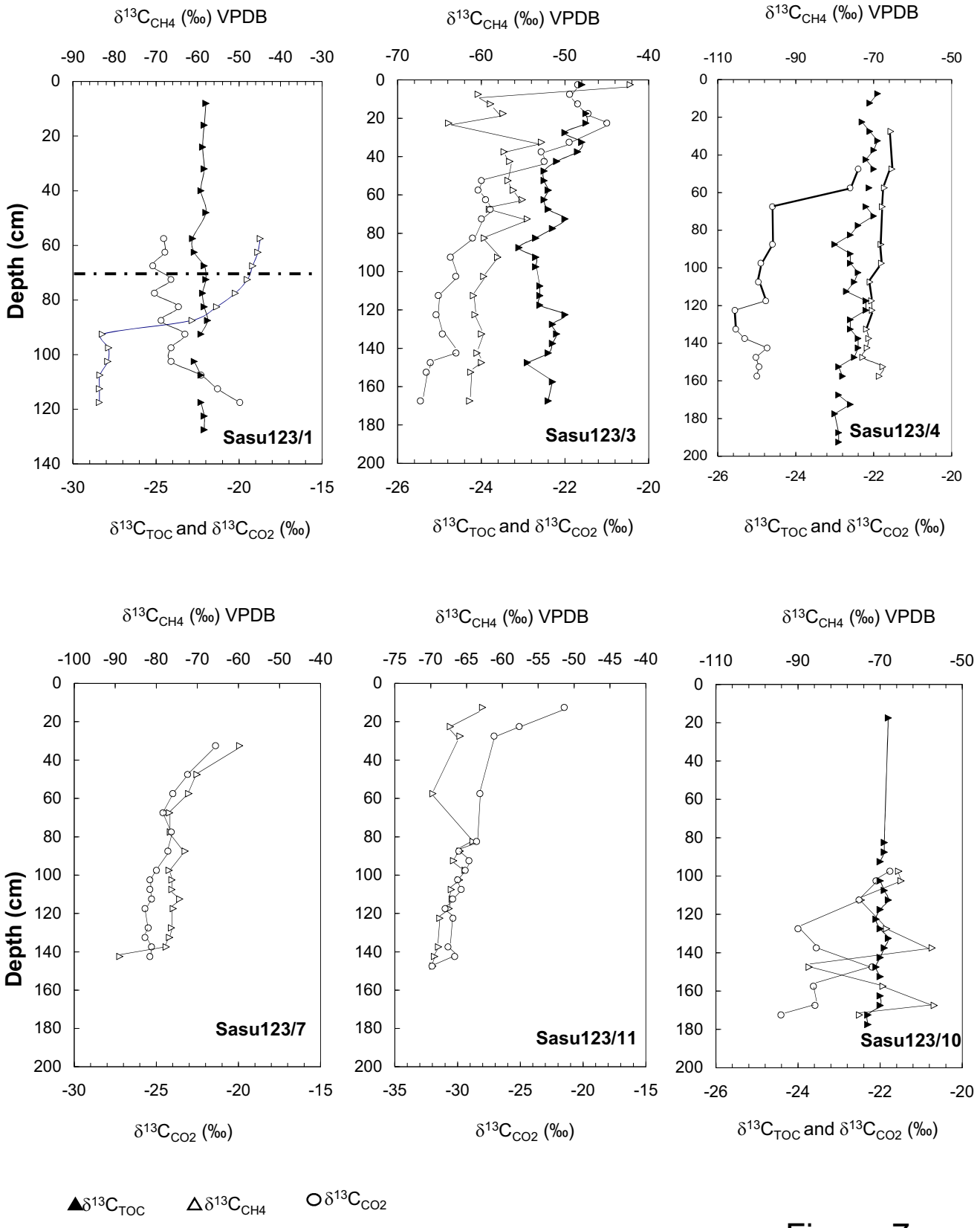

Figure-7

Figure

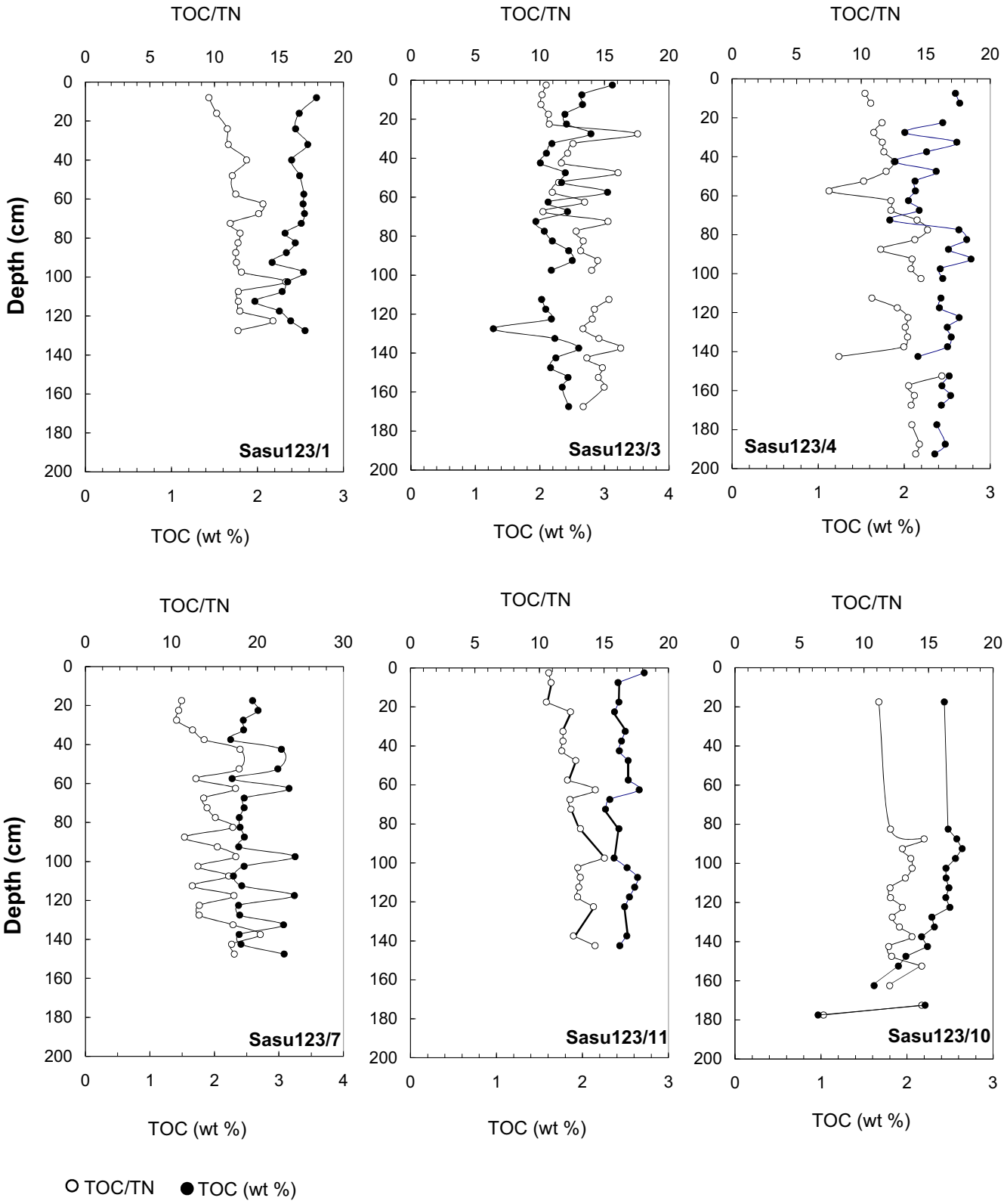

Figure-8

Figure

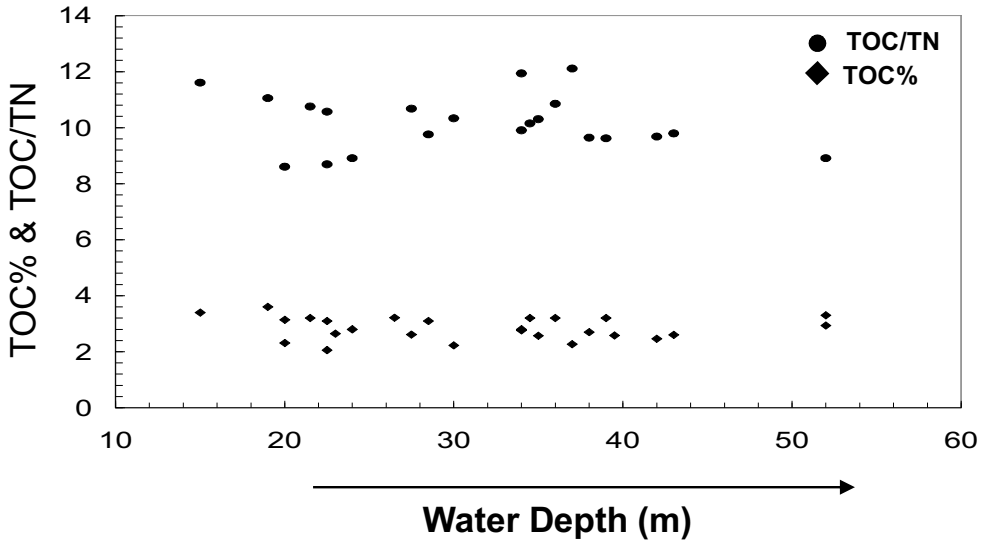

Figure 9

Table-1

Core Number	Latitude	Longitude	Water Depth (m)
Sasu 123/1	15° 7.19' N	73° 54.14' E	14.7
Sasu123/3	15° 4.29' N	73° 52.31' E	20.5
Ssu123/4	15° 3.46' N	73° 50.26' E	26
Sasu123/7	15° 2.27' N	73° 50.85' E	26.5
Sasu123/11	15° 5.01 N	73° 47.08 E	32
Sasu123/10	15° 0.88' N	73° 43.19' E	47
Sasu106/5	15° 5.63' N	73° 53.84' E	16.3
Sasu106/8	15° 4.02' N	73° 49.2' E	29

Table-2

Sasu123/1

Depth (cm)	$SO4^{2-}$ (mM)	CH_4(PPM)	TA (mM)	NH_4^- (µM)	PO_4^{3-} (µM)	TOC(wt%)	TOC/TN	$\delta C^{13}CH_4$	$\delta C^{13}CO_2$	δC^{13}TOC
8			7.4	1102.1		2.7	9.6			-22
16	17.4			873.0	57.3	2.5	10.2			-22.1
24	14.4			1140.0	60.5	2.4	11.0			-22.2
32	12.0			1405.7	71.1	2.6	11.1			-22.1
40			23.9	1439.7		2.4	12.5			-22.3
48	6.2		20.9	1902.1	57.3	2.5	11.4			-22
57.5	5.4	4.0	20.7	1995.7	56.1	2.5	11.6	-44.9	-24.5	-22.8
62.5	3.9	4.7	22.4	2032.6	63.9	2.5	13.8	-45.5	-24.5	-22.7
67.5	nd	8.0	28.0	2092.2	93.0	2.5	13.4	-46.7	-25.2	-22.1
72.5		7.9	30.6	2214.2	91.4	2.5	11.2	-48.0	-24.1	-22
77.5	nd	11.8	25.4	2350.4	74.5	2.3	12.0	-50.9	-25.1	-22.2
82.5	nd	12.3	30.6	2293.6	99.2	2.4	11.8	-55.4	-23.7	-22.1
87.5	nd	22.9	32.2	2404.3	116.4	2.3	11.7	-61.3	-24.7	-21.9
92.5	nd	217.9	31.5	2088.7	116.7	2.2	11.7	-82.9	-23.3	-22.3
97.5		151.6	28.2	2329.8	84.5	2.5	12.1	-81.4	-24.1	
102.5	nd	47.8	34.0	2294.3	107.7	2.4	15.5	-81.6	-24.1	-22.7
107.5	nd	329.9	31.0	2400.7	87.0	2.3	11.8	-83.5	-22.3	-22.3
112.5		277.4	30.1	2478.7	79.8	2.0		-83.6	-21.3	
117.5		530.9	28.8	2542.6	66.4	2.3	12.0	-83.6	-20.0	-22.3
122.5	nd		33.9	2351.1	124.8	2.4	14.5			-22.1
127.5			33.6	2450.4	90.5	2.6	11.8			-22.1

Sasu 123/3

Depth (cm)	$SO4^{2-}$ (mM)	CH_4(PPM)	TA (mM)	NH_4^- (µM)	PO_4^{3-} (µM)	TOC(wt%)	TOC/TN	$\delta C^{13}CH_4$	$\delta C^{13}CO_2$	δC^{13}TOC
2.5	28.9	2.5	4.8	468.2	0.4	3.1	10.5	-42.2	-21.7	-21.6
7.5	29.1	2.6	6.4	371.6	1.0	2.6	10.2	-60.4	-21.9	
12.5	26.9		6.0	246.2	1.3	2.7	10.1	-58.9	-21.7	
17.5	31.1	2.6	5.5	432.9	1.1	2.4	10.7	-57.4	-21.5	-21.5
22.5	30.4	2.7	5.3	483.5	1.4	2.4	10.7	-63.9	-21.0	-21.5
27.5	33.0		5.4	664.9	1.2	2.8	17.6			-22.0
32.5	31.9		5.9	633.1	2.1	2.2	12.6	-52.8	-21.9	-21.6
37.5		3.4	7.4	489.4	2.6	2.1	12.1	-57.3	-22.6	-21.7
42.5	29.0		7.0	548.3	1.3	2.0	11.7	-56.6	-22.5	-22.2
47.5	27.0		7.8	542.4	1.7	2.4	16.1			-22.5
52.5	25.1	4.5	8.9	613.1	2.2	2.3	11.4	-56.8	-24.0	-22.5
57.5		3.9	9.6	615.4	2.8	3.0	11.0	-56.2	-24.1	-22.4
62.5	25.3		10.2	790.9	2.7	2.1	13.5	-55.1	-23.9	-22.5
67.5	22.2	4.0	11.8	765.0	3.9	2.4	10.2	-59.0	-23.8	-22.4
72.5	23.0		10.7	765.0	1.9	1.9	15.3	-54.5	-24.0	-22.0
77.5			11.0	885.2	2.7	2.1	12.8			-22.3
82.5	18.6	6.6	13.9	938.2	3.4	2.2	13.3	-59.6	-24.2	-22.7
87.5	18.5		14.8	986.5	3.6	2.4	13.2			-23.1
92.5		7.0	15.6	946.4	4.8	2.5	14.5	-58.1	-24.7	-22.7
97.5	15.2		15.3	1053.6	2.5	2.2	14.0			-22.7
102.5	13.3	8.2	16.5	1119.6	3.9			-59.7	-24.6	
107.5	14.7		14.6	1101.9	4.1					-22.6
112.5		10.5	17.8	1183.2	4.1	2.0	15.3	-60.9	-25.0	-22.6
117.5	12.1		15.3	1177.3	3.5	2.1	14.2			-22.6
122.5		11.5	18.0	1231.4	4.6	2.2	14.1	-60.8	-25.1	-22.0
127.5			18.5	1262.1		1.3	13.3			-22.3
132.5	8.8	9.8	21.1	1288.0	4.8	2.2	14.6	-60.0	-24.9	-22.2
137.5			20.6	1311.5	5.3	2.6	16.3			-22.3
142.5	7.6	12.2	23.0	1324.5	5.9	2.2	13.6	-60.5	-24.6	-22.4
147.5	6.4	12.9	22.5	1311.5	5.8	2.2	14.8	-60.0	-25.2	-22.9
152.5	5.7	13.0	22.2		6.6	2.4	14.5	-61.3	-25.3	
157.5			22.1	1348.1	5.3	2.3	15.0			-22.3
167.5	5.4	17.6	23.8	1359.8	7.5	2.4	13.4	-61.4	-25.5	-22.4

Sasu 123/4

Depth (cm)	$SO4^{2-}$ (mM)	CH_4(PPM)	TA (mM)	NH_4^- (µM)	PO_4^{3-} (µM)	TOC(wt%)	TOC/TN	$\delta C^{13}CH_4$	$\delta C^{13}CO_2$	$\delta C^{13}TOC$
7.5	26.6		2.6	209.2	1.8	2.6	10.3			-21.9
12.5	25.8		3.1	115.6	5.2	2.6	10.7			-22.1
17.5	25.5		2.8	199.3						
22.5	25.3		3.4	175.2	9.8	2.4	11.6			-22.3
27.5	25.0	2.8	3.6	246.1	13.5	2.0	11.0	-65.6	-19.7	-22.1
32.5	24.2		4.4	315.6	13.5	2.6	11.6			-21.9
37.5	23.7		5.0	372.3	17.8	2.3	11.8			-22.0
42.5			5.5	458.9	18.7	1.9	12.6			-22.2
47.5	22.0	5.1	6.1	529.8	20.9	2.4	11.9	-65.3	-22.4	-22.0
52.5	21.0		6.4	552.5	24.4	2.1	10.2			
57.5	18.4	4.4	7.4	644.7		2.1	7.5	-67.3	-22.6	-22.1
62.5	20.0		7.9	697.2		2.0	12.3			
67.5	16.0	7.0	7.9	738.3	24.7	2.2	12.3	-67.8	-24.6	-22.2
72.5	18.5		8.8	850.4	24.7	1.8	14.3			-22.0
77.5	17.0		9.8	898.6	31.2	2.6	15.1			-22.4
82.5	16.3		10.2	982.3	33.8	2.7	14.2			-22.6
87.5	15.9	7.5	10.2	1057.4	31.2	2.5	11.5	-68.1	-24.6	-23.0
92.5	14.0		10.5	1112.8	28.1	2.8	13.9			-22.6
97.5	14.6	6.8	12.4	968.8	28.7	2.4	13.9	-68.0	-24.9	-22.6
102.5	14.2		11.5	1011.3	32.9	2.4	14.6			-22.4
107.5	12.7	6.4	13.2	1014.2	28.9			-70.9	-25.0	-22.5
112.5			15.5	1306.4	30.9	2.4	10.8			-22.7
117.5	9.5	4.8	11.6	1102.1	35.8	2.4	12.8	-70.5	-24.8	-22.2
122.5	11.2	4.8	13.4	1102.1	30.7	2.6	13.6	-70.4	-25.6	-22.2
127.5	10.7	4.7	13.2	1204.3	33.8	2.5	13.4			-22.6
132.5	9.7	4.3	14.9	1258.2	29.2	2.5	13.6	-71.8	-25.5	-22.6
137.5	10.2	7.0	15.0	1309.2	28.9	2.5	13.3	-71.3	-25.3	-22.4
142.5	9.7	5.5	14.1	1289.4	30.4	2.2	8.3	-71.7	-24.7	-22.4
147.5		7.7						-72.8	-25.0	-22.5
152.5	7.1	6.2	15.8	1590.1	34.4	2.5	16.2	-67.7	-24.9	-22.9
157.5	5.1		18.0	1496.5	32.9	2.4	13.7	-68.6	-25.0	-22.8
162.5	4.7		18.2	1507.8	36.9	2.5	14.1			
167.5	3.8		19.9	1567.4	29.8	2.4	13.9			-22.9
172.5										-22.6
177.5	2.3		19.6	1609.9	30.9	2.4	13.9			-23.0
187.5	3.3		19.1	1689.4	32.9	2.5	14.5			-22.9
192.5	2.3		20.2	1686.5	32.4	2.4	14.2			-22.9

Sasu 123/7

Depth (cm)	$SO4^{2-}$ (mM)	CH_4(PPM)	TA (mM)	NH_4^- (µM)	PO_4^{3-} (µM)	TOC(wt%)	TOC/TN	$\delta C^{13}CH_4$	$\delta C^{13}CO_2$
17.5	29.8		4.8	318.9	8.8	2.6	11.2		
22.5	29.2		4.0	345.4	8.5	2.7	10.8		
27.5	29.9		5.4	421.2	10.8	2.4	10.6		
32.5	28.2	2.5	6.1	542.7	8.2	2.5	12.4	-59.7	-21.4
37.5	28.5		6.0	607.7	9.5	2.2	13.8		
42.5	27.4		6.6	671.5	13.6	3.0	18.0		
47.5		3.2						-70.1	-23.1
52.5	28.5		8.4	779.8	16.2	3.0	17.9		
57.5	24.5	3.8	8.2	871.2	10.1	2.3	12.8	-72.1	-24.0
62.5	23.0		9.5	962.7	13.0	3.2	17.4		
67.5	21.0	4.6	10.7	1059.0	22.6	2.5	13.7	-76.8	-24.6
72.5	21.0		10.3	962.7	19.7	2.5	14.1		
77.5	21.5	4.4	10.5	1085.4	19.7	2.4		-76.6	-24.1
82.5	20.1		10.5	1085.4	16.2	2.4	17.1		
87.5	20.3	3.9	10.2	1167.3	15.3	2.5	11.5	-73.0	-24.3
92.5	19.0		12.1	1275.6	15.9	2.4	15.3		
97.5	19.0		10.6	1460.9	16.9	3.3	17.5	-76.9	-25.0
102.5	17.9	5.1	13.7	1410.3	24.6	2.5	13.1	-76.2	-25.4
107.5	18.3	4.8	11.4	1487.4	17.2	2.3	16.7	-76.2	-25.4
112.5	15.7	5.8	14.8	1176.1	34.8	2.4	12.4	-74.3	-25.3
117.5	15.8	5.5	15.5	1207.3	36.4	3.2	17.3	-75.9	-25.7
122.5	15.0	7.0	14.4	1240.5	29.1	2.4	13.2		
127.5	14.5	6.8	16.0	1300.8	26.5	2.4	13.2	-76.3	-25.5
132.5	14.0		15.7	1300.8	27.5	3.1	17.2	-76.8	-25.7
137.5	12.9		14.0	1504.4	35.2	2.4	20.3	-77.6	-25.3
142.5	12.6		17.9		42.5	2.4	17.0	-88.9	-25.4
147.5						3.1	17.3		

Sasu 123/11

Depth (cm)	$SO4^{2-}$ (mM)	CH_4(PPM)	TA (mM)	NH_4^- (µM)	PO_4^{3-} (µM)	TOC(wt%)	TOC/TN	$\delta C^{13}CH_4$	$\delta C^{13}CO_2$
2.5	28.5		2.6	91.4	3.7	2.7	10.7		
7.5	29.6		2.9	39.5	10.1	2.4	10.9		
12.5	28.8		4.2	220.3	12.4			-62.8	-21.5
17.5	29.1		5.7	435.3	15.3	2.4	10.5		
22.5	27.6	3.8	6.4	361.6	10.4	2.4	12.4	-67.3	-25.1
27.5	26.7	4.5	7.6	492.5	18.5			-65.9	-27.1
32.5	23.9	6.6	8.1	583.9	20.4	2.5	11.8		
37.5	22.4		9.2	637.9	22.6	2.5	11.8		
42.5			9.5	706.5	17.2	2.4	11.7		
47.5	21.3		10.9	837.4	24.9	2.5	12.8		
52.5	20.2								
57.5	15.9	7.1	11.9	816.6	24.6	2.5	12.2	-69.7	-28.2
62.5	17.5		11.2	864.4	21.0	2.7	14.3		
67.5	16.5		11.9	920.5	23.9	2.3	12.4		
72.5	16.3		12.0	716.9	18.5	2.3	12.4		
78	15.7		12.6	1207.3	18.5				
82.5	13.8	2.7	14.3	1009.9	26.8	2.4	13.2	-64.1	-28.5
87.5	14.6	10.7	13.2	1078.4	22.3			-65.9	-29.9
92.5	14.1	12.7						-66.8	-29.1
97.5	12.6	2.9	14.3	1016.1	22.0	2.4	15.0	-65.2	-29.4
102.5	10.8	11.6	17.2	1059.7	27.5	2.5	13.0	-66.0	-30.0
107.5	9.9	13.1	16.2	1088.8	18.5	2.6	13.2	-67.1	-29.7
112.5	9.0		17.9	1357.9	35.2	2.6	13.0	-67.0	-30.4
117.5	8.5	16.9	18.7	1221.8	34.5	2.5	12.9	-67.4	-31.0
122.5	8.7	12.7	17.3	1242.6	26.2	2.5	14.2	-68.7	-30.4
129	6.9		18.5	1126.2	33.2				
134	6.4		18.7	1440.0	28.4				
137.5	5.3	13.3	18.6	1354.8	35.5	2.5	12.6	-68.9	-30.8
142.5	5.8	19.4	18.3	1359.0	37.1	2.4	14.3	-69.5	-30.2
147.5	4.8	13.3	19.8	1315.3	36.4			-69.7	-32.0
152.5	5.1		21.2	1369.4	44.2				

Sasu 123/10

Depth (cm)	$SO4^{2-}$ (mM)	CH_4(PPM)	TA (mM)	NH_4^- (µM)	PO_4^{3-} (µM)	TOC(wt%)	TOC/TN	$\delta C^{13}CH_4$	$\delta C^{13}CO_2$	$\delta C^{13}TOC$
17.5	30.4		2.9	184.9	4.5	2.4	11.1			-21.8
82.5	23.5		7.7	802.1	9.5	2.5	12.0			-21.9
87.5	23.4		7.8	716.9	8.0	2.6	14.7			-21.9
92.5	23.7		7.9	827.0	6.7	2.6	13.0			-22.0
97.5	20.6	3.0	8.5	675.3	14.2	2.6	13.6	-65.5	-21.8	
102.5	23.7		8.0	841.6	8.6	2.5	13.7	-64.9	-22.1	-22.0
107.5	22.4	2.9	8.4	928.8	10.2	2.5	13.2			-21.9
112.5	24.0		8.2	895.6	7.3	2.5	12.0	-74.6	-22.5	-21.8
117.5	22.0	2.6	8.5	839.5	10.5	2.5	12.0			-22.0
122.5			7.2	712.7	8.0	2.5	13.0			-22.1
127.5	23.6	3.9	8.7	906.0	9.2	2.3	12.2	-68.4	-24.0	-22.0
132.5	23.5		8.7	849.9	9.0	2.3	12.7			-21.8
137.5	24.1	3.5	9.0	804.2		2.2	13.7	-57.3	-23.6	-21.9
142.5			8.4			2.2	11.9			-22.0
147.5	22.1	3.2	8.3	783.4		2.0	12.1	-87.3	-22.2	-22.1
152.5	21.8		9.5	854.0	8.9	1.9	14.5			-22.0
157.5		3.8			13.6			-69.3	-23.6	
162.5			8.8	897.7	7.3	1.6	12.0			-22.0
167.5	20.8	2.6	8.5	854.0	10.8	2.8		-56.9	-23.6	
172.5	23.0		9.2	768.8	7.3	2.2	14.5	-75.0	-24.4	-22.3
177.5	20.1	2.7	9.7		6.1	1.0	6.9			-22.3